The Effect of Gradual Fluorination on the Properties of F_nZnPc Thin Films and F_nZnPc/C_{60} Bilayer Photovoltaic Cells

Michael Brendel, Stefan Krause, Andreas Steindamm, Anna Katharina Topczak, Sudhakar Sundarraj, Peter Erk, Steffen Höhla, Norbert Fruehauf, Norbert Koch, and Jens Pflaum*

Motivated by the possibility of modifying energy levels of a molecule without substantially changing its band gap, the impact of gradual fluorination on the optical and structural properties of zinc phthalocyanine (F_nZnPc) thin films and the electronic characteristics of F_nZnPc/C_{60} (n = 0, 4, 8, 16) bilayer cells is investigated. UV–vis measurements reveal similar Q- and B-band absorption of F_nZnPc thin films with n = 0, 4, 8, whereas for $F_{16}ZnPc$ a different absorption pattern is detected. A correlation between structure and electronic transport is deduced. For F_4ZnPc/C_{60} cells, the enhanced long range order supports fill factors of 55% and an increase of the short circuit current density by 18%, compared to $ZnPc/C_{60}$. As a parameter being sensitive to the organic/organic interface energetics, the open circuit voltage is analyzed. An enhancement of this quantity by 27% and 50% is detected for F_4ZnPc- and F_8ZnPc-based devices, respectively, and is attributed to an increase of the quasi-Fermi level splitting at the donor/acceptor interface. In contrast, for $F_{16}ZnPc/C_{60}$ a decrease of the open circuit voltage is observed. Complementary photoelectron spectroscopy, external quantum efficiency, and photoluminescence measurements reveal a different working principle, which is ascribed to the particular energy level alignment at the interface of the photoactive materials.

1. Introduction

Progress in the field of organic photovoltaics has been tremendous during the past decade, leading to today's power conversion efficiencies of 10% for polymeric single junction cells and 12% for small molecule tandem solar cells.[1,2]

As a key functional unit, organic photovoltaic cells (OPVCs) contain a donor/acceptor (D/A) heterojunction, which provides the driving force for dissociation of photogenerated, strongly Coulomb-bound electron–hole pairs, so-called excitons. Moreover, the respective energy levels of the donor and acceptor at the common interface are crucial for the overall open circuit voltage (V_{oc}) of planar heterojunction (PHJ) devices. The effective band gap ($E_{g,eff}$) between the highest occupied molecular orbital (HOMO) of the donor and the lowest unoccupied molecular orbital (LUMO) of the acceptor defines the upper limit of the quasi-Fermi level splitting and thus of V_{oc}.[3,4] Considering the effective doping of the donor and acceptor layers upon dissociation of the photogenerated electron–hole pairs, the open circuit voltage for an idealized p/n-junction reads

$$e \cdot V_{oc} \approx E_{g,eff} + k_B T \cdot \ln\left(\frac{n_n \cdot n_p}{N_{LUMO\ acceptor} \cdot N_{HOMO\ donor}}\right) \quad (1)$$

Here, k_B represents the Boltzmann constant, T the temperature, $(n_n/N_{LUMO\ acceptor})$ and $(n_p/N_{HOMO\ donor})$ are the relative electron and hole doping concentrations of the acceptor and the donor layer. For various organic compounds the loss term △,

M. Brendel, A. Steindamm, A. K. Topczak, Prof. J. Pflaum
Experimental Physics VI, Julius-Maximilians University
Am Hubland, 97074 Würzburg, Germany
E-mail: michael.brendel@physik.uni-wuerzburg.de
Dr. S. Krause, Prof. N. Koch
Helmholtz-Zentrum für Materialien und Energie GmbH
Albert-Einstein-Str.16, 12489 Berlin, Germany
Dr. S. Krause, Prof. N. Koch
Humboldt-Universität zu Berlin
Institut für Physik
Newtonstr. 15, 12489 Berlin, Germany
Dr. S. Sundarraj
BASF South East Asia Pte Ltd., No. 61
Science Park Road, # 03-01 The Galen
Singapore Science Park II, Singapore 117525, Singapore
Dr. P. Erk
BASF SE
GVE/E-J542, 67056 Ludwigshafen, Germany
S. Höhla, Prof. N. Fruehauf
Institut für Großflächige Mikroelektronik
Allmandring 3b, 70569 Stuttgart, Germany
Prof. J. Pflaum
Bavarian Center for Applied Energy Research e.V. (ZAE Bayern)
Am Galgenberg 87, 97074 Würzburg, Germany

DOI: 10.1002/adfm.201404434

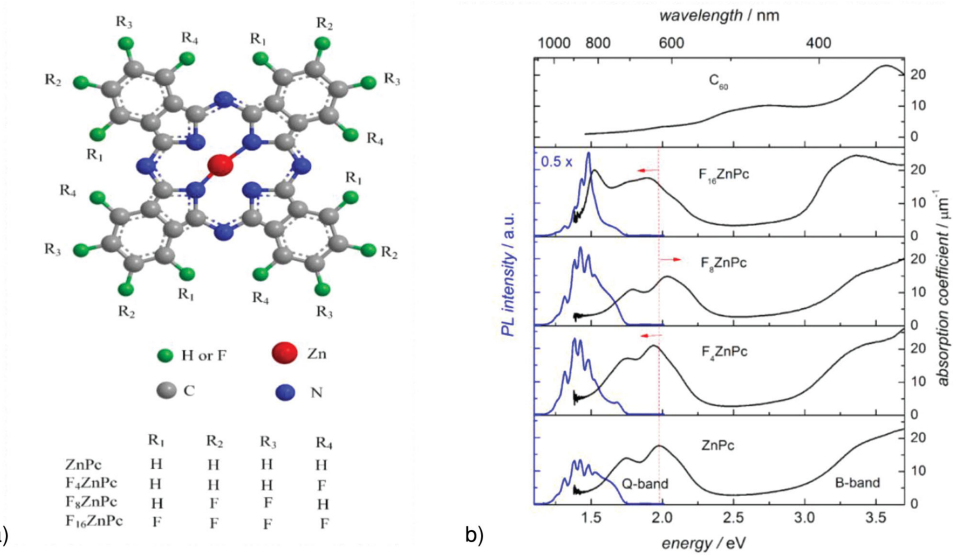

Figure 1. a) Structural motif of the employed F_nZnPcs and their respective ligand configuration. b) Spectrally resolved photoluminescence (blue curves) and absorption (black curves) of 40 nm F_nZnPc thin films, together with the complementary absorption spectra of C_{60} (upper graph). Red arrows indicate the spectral shifts of the absorption, caused by fluorination.

which is attributed to radiative and nonradiative recombination processes, was estimated to be 0.4–0.6 eV at room temperature under AM 1.5 standard illumination conditions.[5–8] Thus, Equation (1) can be expressed as

$$e \cdot V_{oc} \approx E_{g,eff} - \Delta \quad (2)$$

To develop a fundamental understanding on the heterojunction characteristics and their dependence on the microscopic conditions, tuning of the energy level positions has been considered a suitable strategy.[9] One way to tackle this challenge is the use of materials with defined chemical modification. In this regard, phthalocyanines are promising candidates because of their numerous possibilities for chemical substitution, such as the central metal atom or the hydrogen atoms of the ligand, without substantially affecting their molecular shape or energy gap.[10,11] The chemical structure of fluorinated zinc phthalocyanines (F_nZnPc), which constitute the compounds of interest in this study, is shown in **Figure 1**a. By increasing the degree of fluorination, the HOMO and LUMO levels are shifted toward lower energies, without significant change of the corresponding band gap.[12] This energetic staircase-behavior upon gradual fluorination has been qualitatively verified by semiempirical calculations, apart from some deviations between the absolute HOMO level positions.[12,13]

In this contribution, we utilize zinc phthalocyanines to investigate the impact of gradual fluorination on the photophysical properties of F_nZnPc thin films and F_nZnPc/C_{60} (n = 0, 4, 8, 16) bilayer cells. The choice of materials is motivated by their complementary spectral absorption in the visible, confirmed by our optical and external quantum efficiency (EQE) measurements, and by short circuit current densities (j_{sc}) of up to 12 mA cm^{-2}, reported for bulk-heterojunction solar cells.[14] Moreover, in comparison to other metal phthalocyanines, the frontier orbital configuration of ZnPc is beneficial for the performance of bilayer cells in combination with C_{60}.[11] By X-ray diffraction (XRD) we are able to evidence the impact of fluorination on the thin film morphology and to correlate the good transport properties, indicated by fill factors of up to 55% in case of F_4ZnPc/C_{60} cells, with the underlying structural order.

Additionally, in comparison to unsubstituted ZnPc/C_{60}, we demonstrate a significant V_{oc} increase by 27% and 50% for F_4ZnPc/C_{60} and F_8ZnPc/C_{60} bilayer devices, respectively. In general, this trend in V_{oc} can be attributed to an increase of the effective band gap at the D/A interface, as confirmed by ultraviolet photoelectron spectroscopy (UPS), whereas for F_{16}ZnPc/C_{60} the interface is proven to be mainly photoinactive.

2. Results and Discussion

2.1. Optical Properties of F_nZnPc (n = 0, 4, 8, 16) Thin Films

Phthalocyanines are known to have two distinct absorption bands in the UV–vis-spectral region. The so-called Q-band originates from an a_{1u} to e_g transition, in analogy to the π–π^* excitation of porphyrins. This Q-band has a doublet at 1.72 and 2.00 eV, resulting from a lift of the excited state degeneracy by vibronic coupling, termed Davydov-splitting. The second transition band, also called B-band, corresponds to the Soret- or γ-band in porphyrins. This band originates from transitions between the a_{2u} and b_{1u} orbitals and the excited e_g state with the strongest absorption band located at 3.65 eV.[15,16]

To study the impact of fluorination on the neat optical properties, we investigated 40 nm thick F_nZnPc (n = 0, 4, 8, 16) films sublimed onto glass substrates at room temperature. As shown in Figure 1b, F_nZnPcs absorb in a spectral range complementary to C_{60}. The overall shape of the absorption spectra is remarkably similar for ZnPc, F_4ZnPc, and F_8ZnPc, confirming both, the conservation of the relative energy level positions

viz. the optical band gap as well as of the local crystallographic symmetry upon fluorination. A broad but structured absorption peak is located between 1.75 and 1.79 eV accompanied by an additional absorption shoulder at higher energy between 1.94 and 2.04 eV. These spectral features have been assigned to the Davydov-splitted Q-band absorption of the α-phase of crystalline metal phthalocyanines.[12,15,17] In addition, the broad B-band absorption is detected with an onset at 3 eV and a characteristic maximum around 3.4 eV.

Noticeably, with reference to unsubstituted ZnPc the Q-band absorption of F_4ZnPc appears red-shifted by 40 meV, whereas for F_8ZnPc it appears blue-shifted by 50 meV, which is indicated by red arrows in Figure 1b. Despite their small amplitudes these energy shifts render reproducible as will be demonstrated by EQE data below and can be attributed to slight modifications of the transition dipole alignment and the intermolecular coupling upon fluorination. In contrast to its homologs, F_{16}ZnPc shows a different absorption spectrum. Besides a strong peak at 1.89 eV and a peak of smaller intensity at 1.75 eV, both resembling the energy spacing observed for the three previous compounds, an additional intense peak occurs in the near infrared (NIR) spectral region at 1.54 eV. Moreover, a slight broadening of the Q- and B-band is observed for the F_{16}ZnPc layer. We ascribe these differences in the absorption characteristics to changes of the intermolecular packing in F_{16}ZnPc thin films with respect to those of the other F_nZnPc compounds, providing first evidence for the existence of a different crystalline structure.[12,17]

Though no crystallographic data on F_{16}ZnPc polymorphs can be found in literature, the perfluorinated F_{16}CuPc equivalent is known to crystallize in two different packings, the so called β-phase and $\beta_{bilayer}$-phase.[18] For the β-phase, the stacking within the (ab)-plane shows a herringbone arrangement with two molecules per unit cell, whereas the $\beta_{bilayer}$-phase contains only one molecule per unit cell and crystallizes in a face-on configuration along the (ab)-plane.[18] As a result of the different packings, both crystal structures show distinct absorption characteristics associated with absorption peaks at 1.54 eV for the β-phase polymorph and at 1.89 and 1.77 eV for the $\beta_{bilayer}$-phase.[9] The agreement between the spectral positions of these absorption peaks with those experimentally observed for our F_{16}ZnPc thin film samples speaks in favor of the existence of similar polymorphs in the latter.

Along with the absorption, the complementary photoluminescence (PL) spectra of F_nZnPc thin films (635 nm excitation wavelength) are shown in Figure 1b. Broad PL bands appear between 1.20 and 1.75 eV and can be related to emission originating from the Q-band.[19] The shapes of the PL spectra of ZnPc, F_4ZnPc, and F_8ZnPc resemble each other. The emission maxima located at 1.42 eV result in Stokes shifts of 2600–2800 cm^{-1}. In contrast, F_{16}ZnPc shows a different PL signature. Especially the peak intensity at 1.48 eV appears to be exceptionally high and the related Stokes shift is reduced to 380 cm^{-1}. Despite broader absorption of F_{16}ZnPc, the width of the PL band renders almost identical to that of the other F_nZnPcs. This observation can be rationalized by the fact that according to Kasha's rule, emission always occurs from the energetically lowest lying, dipole-allowed excited state which is expected to refer to the energetically lowest lying Davydov-component in F_{16}ZnPc crystalline thin films.

2.2. Morphological Studies of F_nZnPc (n = 0, 4, 8, 16) Thin Films

As the optical and even more the electronic transport properties are related to the structural characteristics on microscopic length scales, we have analyzed the degree of crystallinity and the texture of the F_nZnPc layers by means of X-ray diffraction in Bragg–Brentano geometry. **Figure 2**a depicts the diffraction spectra, which refer to the momentum transfer, q_z, along the surface normal and thus illustrate the out-of-plane crystalline ordering. The first order diffraction peak for unsubstituted ZnPc at q_z = 0.48 $Å^{-1}$ corresponds to a lattice spacing of d_{ZnPc} = 13.0 Å and is in good agreement with data of the α-phase crystal structure with edge-on orientation of the molecules.[11,20]

With increasing degree of fluorination the Bragg peaks are shifted to lower q_z-values and vice versa, yielding larger lattice spacings as shown in Figure 2b (d_{F4ZnPc} = 13.4 Å,

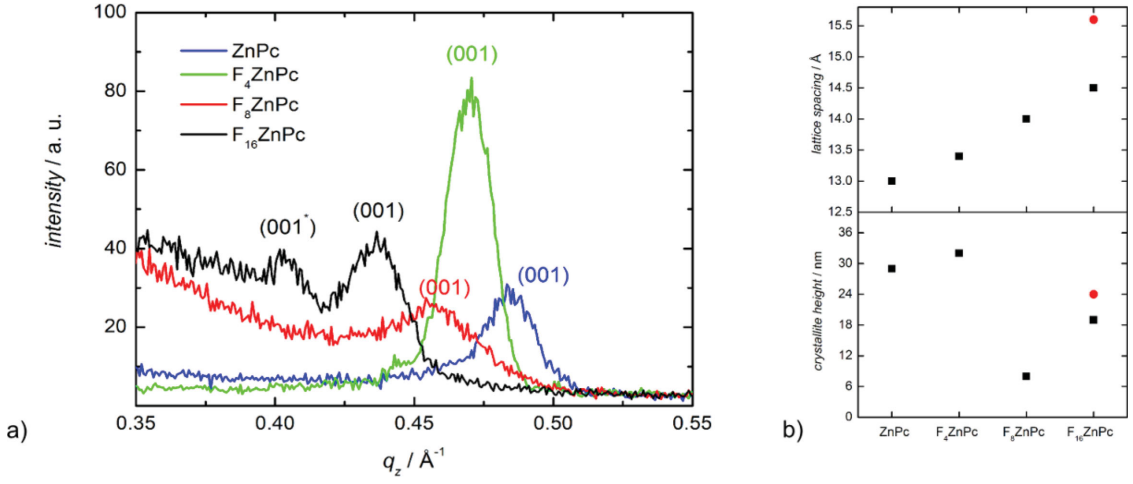

Figure 2. a) X-ray diffraction spectra of 40 nm thick F_nZnPc (n = 0, 4, 8, 16) films. b) Corresponding (001) lattice spacings and crystallite heights. Red symbols represent the values of the corresponding F_{16}ZnPc polymorph.

d_{F8ZnPc} = 14.0 Å, $d_{F16ZnPc}$ = 14.5 Å). As a similar tendency was reported for CuPc and F_{16}CuPc (d_{CuPc} = 12.4 Å, $d_{F16CuPc}$ = 14.4 Å),[9] the increase in lattice spacing can be attributed to the stronger repulsion of the electronegative fluorine groups, changing the interaction between molecules for the different compounds and thereby, altering the subtle balance between the substrate–molecule interaction and the intermolecular packing energy. This results in a different molecular tilting with respect to the surface normal and therefore, in the observed changes of the effective out-of-plane lattice constant. Moreover, the increase in lattice spacing is supported by the different sizes of the F_nZnPc molecules, caused by the increasing van der Waals radii upon fluorination. Finally, as already suggested by the UV–vis data, an additional diffraction peak appearing at q_z = 0.41 Å^{-1} for the F_{16}ZnPc thin film confirms the existence of a second crystalline phase with an (001)* lattice spacing of 15.6 Å.

The implementation of organic thin films in photovoltaic devices requires a sufficiently good exciton diffusion and charge carrier transport, both correlating with the degree of structural order along the surface normal.[21–23] Therefore, by means of the Scherrer equation, the out-of-plane crystallite height h along the transport direction for excitons and charge carriers is calculated

$$h = \frac{0.94 \cdot \lambda}{\cos\left(\frac{2\theta}{2}\right) \cdot \Delta\theta} \quad (3)$$

Here, λ represents the incident X-ray wavelength of the Cu $K_{\alpha 1}$ radiation, 2θ the angular position of the Bragg peak, and $\triangle\theta$ its full width at half maximum. As shown in Figure 2b we ascertain a strong influence of fluorination on the crystallite height of the F_nZnPc films. According to these data, the best transport properties are expected for ZnPc and F_4ZnPc thin films with crystalline domains extending to about 80% of the nominal film thickness. In contrast, the distorted textures of the F_8ZnPc and F_{16}ZnPc films, indicated by smaller grain sizes of only 20% and 50% of the nominal layer thickness, respectively, impose stronger constraints on exciton and charge carrier motion as will be confirmed below by their impact on fill factor and short circuit current density of the PHJ cells. Remarkably, the crystallite heights of the two F_{16}ZnPc polymorphs are similar in size and moreover, add up to the nominal film thickness of 40 nm. Therefore, it can be rationalized, that the two structural phases grow mainly on-top of each other, which has decisive consequences for the F_{16}ZnPc thicknesses chosen for thin film organic electronics.

2.3. Ultraviolet Photoelectron Spectroscopy on F_nZnPc/C_{60} (n = 0, 4, 8, 16) Bilayers

Since macroscopic solar cell parameters are essentially determined by the energetics at the donor/acceptor heterojunction, UPS measurements were carried out, to reveal the relevant energy level positions in our photovoltaic bilayer cells. To resemble the device architecture of the photovoltaic cells, thickness-dependent UPS investigations were conducted on F_nZnPc/C_{60} bilayers thermally deposited onto ITO/MoO_3 substrates. Exemplarily, **Figure 3**a depicts UPS valence band (VB) spectra and Figure 3b the secondary electron cutoff (SEC) of an ITO/MoO_3(5 nm)/ZnPc(30 nm)/C_{60}(35 nm) stack resembling the layer thicknesses of the optimized bilayer photovoltaic cells studied afterward. Energy levels were determined by the onset of the peaks and by adding the respective electronic band gap to the HOMO and VB energies, the LUMO and conduction band (CB) positions were determined.[24] Shifts of the SEC refer to changes of the sample work function with respect to the Fermi level E_F and thus hint at the occurrence of an effective interface dipole.

The band diagram across the active layers of our planar heterojunction devices are shown in **Figure 4** for all four

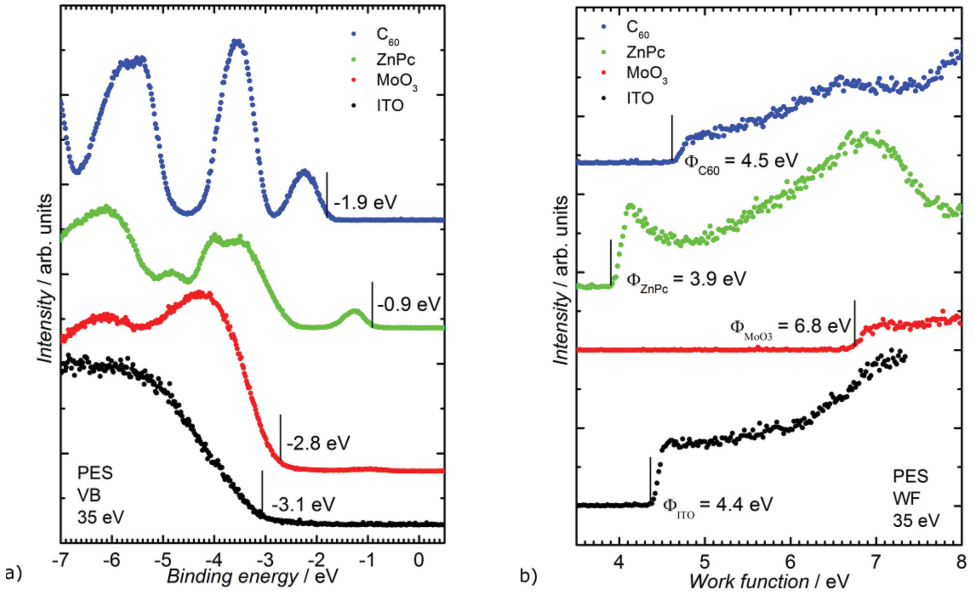

Figure 3. a) Valence band and b) work function scan of the respective final layer thicknesses for the ZnPc/C_{60} heterojunction.

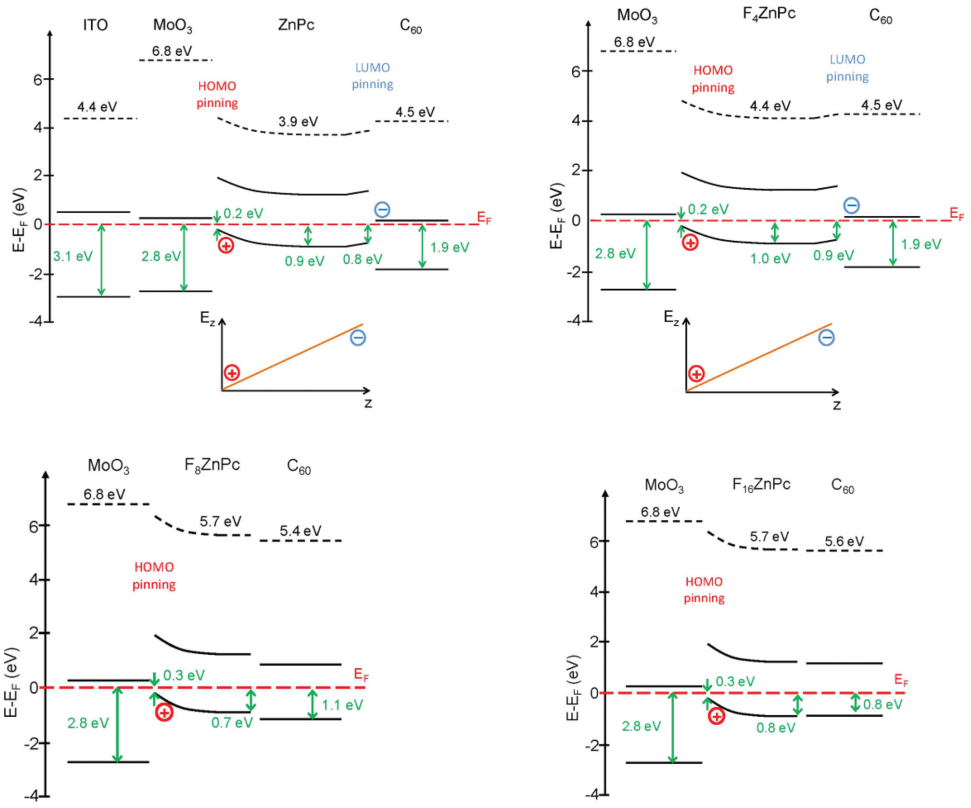

Figure 4. Band alignment diagram in the studied F_nZnPc/C_{60} devices.

donor/acceptor combinations under study. As a general tendency, the ionization energy of the F_nZnPcs is shifted toward higher values with increasing degree of fluorination. Compared to nonfluorinated ZnPc the absolute frontier orbital shift for the perfluorinated phthalocyanine amounts to 1.7 eV. This energetic staircase-behavior is quantitatively similar to values experimentally as well as theoretically determined in literature.[10,12,25]

The high work function MoO_3 layer causes a strong positive charge accumulation at its interface and thus forces all F_nZnPc layers to a strong Fermi level pinning of their HOMO.

At 30 nm film thickness the HOMO position with respect to E_F amounts to 0.9 eV for ZnPc and 1.0 eV for F_4ZnPc. After final deposition of C_{60} the HOMO of these phthalocyanine layers is shifted upward and the C_{60} shows a Fermi level pinning of its LUMO, since the electron affinity of the fullerene exceeds the ionization potential of the donor materials. This pinning is not as strong as at the MoO_3 interface but it leads to an accumulation of negative charge at the $ZnPc/C_{60}$ and F_4ZnPc/C_{60} boundary. The electric field between these negative charges and the positive charges at the MoO_3 interface causes an upward bending of the ZnPc and F_4ZnPc HOMO by 0.1 eV. As can be concluded from Figure 4, upon deposition of C_{60} on ZnPc an upward shift of the SEC and thus of the vacuum level by 0.6 eV occurs, indicating the appearance of an effective interfacial dipole at the donor/acceptor interface. Therefore, the assumption of a common vacuum level for the active organic layers is a priori not justified in these devices.

In case of F_8ZnPc- and $F_{16}ZnPc$-based heterojunctions, their HOMO levels are Fermi level pinned at the MoO_3 interface but then shift downward with increasing thickness. The absolute values of the HOMO position at 30 nm show variations in different experiments and range in the case of F_8ZnPc between 0.7 and 0.9 eV. However, the relative distance between the F_8ZnPc and the C_{60} HOMOs remains constant at 0.4 eV, which confirms the expected vacuum level alignment at the organic/organic interface. The same holds true for $F_{16}ZnPc$, i.e., in both heterostructures no LUMO level pinning for the fullerene is observed.

The occurrence and absence of the C_{60} LUMO level pinning for the differently fluorinated F_nZnPc layers has a distinct impact on the respective energetics at the donor/acceptor interface and consequently influences the macroscopic solar cell characteristics, as will be shown in Section 2.4. Therefore, this case study constitutes a remarkable example for the interplay and the emerging electronic effects upon systematic variation of the energetic properties at otherwise similar donor/acceptor boundaries.

2.4. Electrical Characterization of F_nZnPc/C_{60} (n = 0, 4, 8, 16) OPVCs

2.4.1. External Quantum Efficiency and Photoluminescence Measurements

Before discussing the overall macroscopic performance of the bilayer photovoltaic devices, we now focus on the photophysical properties of the individual molecular components. For this purpose, we correlated the individual contributions of F_nZnPc

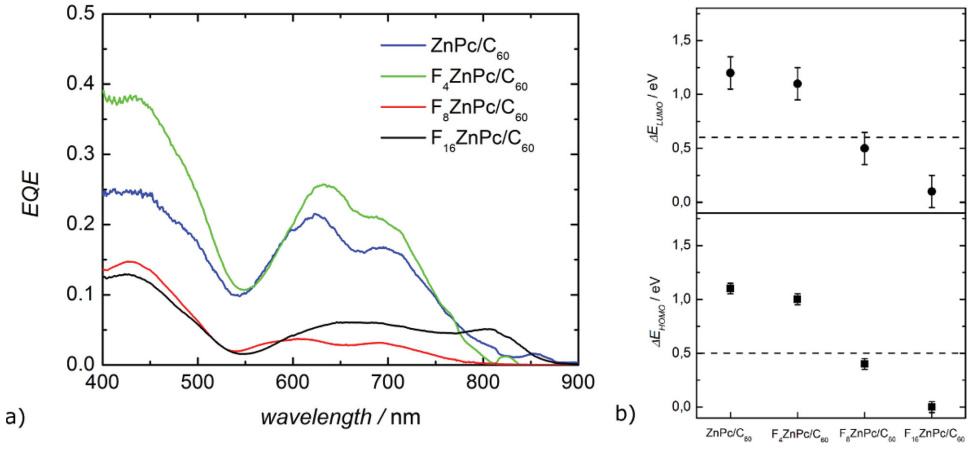

Figure 5. a) EQE of F_nZnPc (30 nm)/C_{60} (35 nm) bilayer OPVCs. EQE measurements were performed without background illumination at an average light intensity for each wavelength step of approx. 10^{-2} mW cm^{-2}. b) HOMO level offset ΔE_{HOMO} and LUMO level offset ΔE_{LUMO} of the different F_nZnPcs with respect to C_{60}. Additionally, the exciton binding energies of C_{60} (bottom) and ZnPc (top) are indicated by dotted lines.[26,27]

and C_{60} to the spectrally resolved photocurrent in our PHJ cells and calculated the EQE, which is shown in **Figure 5**a. Comparing the wavelength-dependent EQE with the absorption coefficients in Figure 1b it becomes evident that in our F_nZnPc/C_{60} (n = 0, 4, 8, 16) bilayer cells both semiconductors contribute to the photogeneration of charge carriers. In the spectral range between 400 and 550 nm, the photocurrent originates predominantly from C_{60}, whereas between 550 and 850 nm it can be mostly assigned to F_nZnPc. Thus, the complementary absorption of F_nZnPc and C_{60} covers a broad spectral range between 400 and 850 nm, as desired.

In agreement with the corresponding UV–vis data of ZnPc, F_4ZnPc, and F_8ZnPc thin films (see Figure 1b), two distinct maxima located at 615 and 700 nm can be identified in the EQE curves of each material combination. Furthermore, the same spectral shifts for the F_4ZnPc-, F_8ZnPc-, and F_{16}ZnPc-based devices are detected as well as an additional maximum in the NIR spectral region at 812 nm for the F_{16}ZnPc/C_{60} bilayer cells.

The extended crystallite size of the F_4ZnPc films supports both, larger exciton diffusion lengths and efficient charge carrier transport to the electrodes, enhancing the EQE by 25% in comparison to ZnPc/C_{60} cells.[21–23] In contrast, the EQE for F_8ZnPc/C_{60} and F_{16}ZnPc/C_{60} is considerably reduced by 70% and 60%.

To achieve a qualitative understanding for this behavior, the energetic positions of the respective HOMO and LUMO levels at the common D/A interface have to be considered (see Figure 4). The energy difference ΔE_{HOMO} between the F_nZnPc and C_{60} HOMO levels at the heterojunction drives the dissociation of photogenerated excitons in C_{60}, as long as this energy difference exceeds the exciton binding energy. Likewise, the energy difference ΔE_{LUMO} between the LUMO levels of F_nZnPc and C_{60} is crucial for the separation of excitons generated within the F_nZnPc layers. In Figure 5b, ΔE_{HOMO} and ΔE_{LUMO} are displayed for the four different F_nZnPc/C_{60} material combinations together with the exciton binding energy in C_{60} ($E_{Bind\ C60}$ = 0.5 eV, lower graph) and in ZnPc ($E_{Bind\ ZnPc}$ = 0.6 eV, upper graph).[15,26,27] It becomes immediately obvious that for ZnPc/C_{60} and F_4ZnPc/C_{60} ΔE_{HOMO} exceeds $E_{Bind\ C60}$, rendering exciton dissociation highly efficient. In a similar manner, the LUMO energy offset ΔE_{LUMO} surpasses the exciton binding energy in F_nZnPc for these devices. For the F_8ZnPc/C_{60} heterojunctions, in contrast, ΔE_{LUMO} and ΔE_{HOMO} lie in the same energy range as the respective exciton binding energies. Hence, dissociation into free charge carriers may be limited. Considering also the lower structural coherence within the donor layer, this results in the observed decrease of the EQE.

According to Figure 5b, there is no sufficient excess energy to accomplish dissociation of photogenerated excitons at the F_{16}ZnPc/C_{60} interface. Nevertheless, a clear photovoltaic response is detected for both absorber materials in Figure 5a. This raises the question about the underlying working mechanism of these solar cells. In literature it is well known that excitons can be dissociated at metal oxide/organic interfaces.[28] Moreover, due to the energy level alignment at the F_{16}ZnPc/C_{60} interface with almost no energetic offset (see Figure 4), it can be rationalized that excitons created in the fullerene phase are transferred to a substantial amount to the phthalocyanine layer and, subsequently, become dissociated at the MoO_3/F_{16}ZnPn interface as well.

To verify this hypothesis the spectrally resolved photoluminescence of ITO/MoO_3/F_nZnPc thin films at 532 nm excitation wavelength was compared to the PL of the corresponding ITO/MoO_3/F_nZnPc/C_{60} heterostructures, i.e., including the fullerene acceptor layer. The upper graph in **Figure 6** shows the influence of the C_{60} acceptor layer on the PL in case of the F_4ZnPc samples. In this spectral range, the PL of C_{60} is very weak (not shown), since radiative transitions are dipole forbidden. Nevertheless, the PL in the measured spectral range was corrected for this contribution by a polynomial fit of second order.

As expected, in presence of the C_{60} acceptor layer, excitons created in F_4ZnPc become dissociated at the D/A interface, hence reducing the PL of the phthalocyanine. The same behavior is detected for the bilayer heterojunctions based on ZnPc and F_8ZnPc (not shown).

The lower graph in Figure 6 illustrates that the C_{60} layer affects the PL of the heterojunction based on the perfluorinated F_{16}ZnPc in an opposite way. In this case, an increase of the PL originating from F_{16}ZnPc is detected in presence of the fullerene. Thus, the working principle of F_{16}ZnPc/C_{60} solar

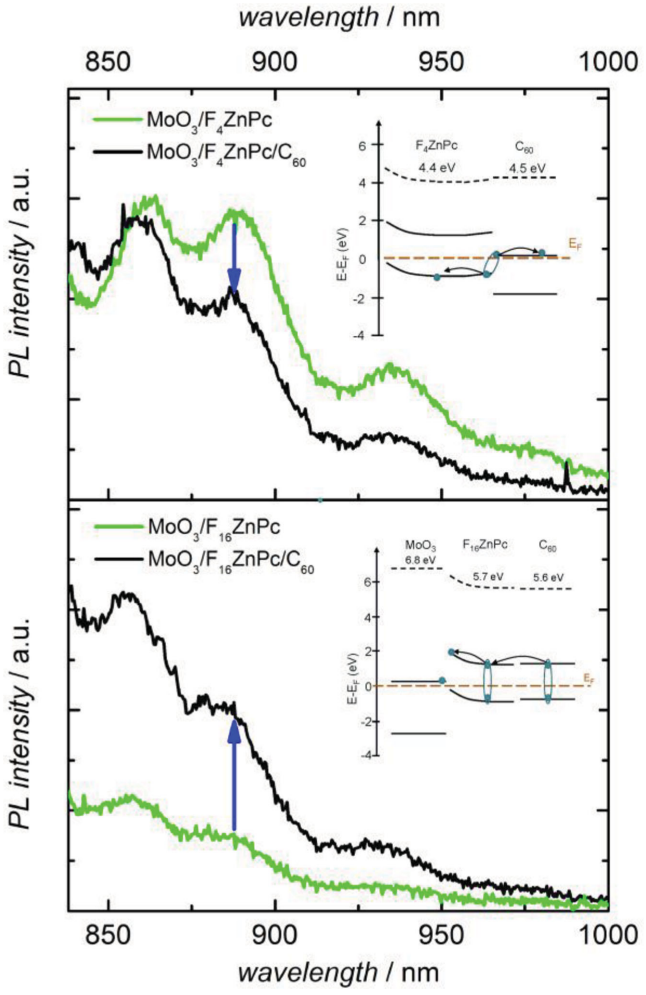

Figure 6. Spectrally resolved PL of ITO/MoO_3/F_nZnPc thin films at 532 nm excitation, compared to the PL of the corresponding heterostructures ITO/MoO_3/F_nZnPc/C_{60}. Upper graph: In presence of the C_{60} acceptor, excitons created in F_4ZnPc get dissociated at the common D/A interface, reducing the PL (indicated by the blue arrow). Lower graph: The C_{60} layer conversely affects the PL of F_{16}ZnPc heterojunctions. An increase of the PL originating from F_{16}ZnPc is detected in presence of the fullerene (indicated by the blue arrow). Insets illustrate the exciton dissociation processes in the respective photovoltaic devices.

cells is fundamentally different in comparison to the other solar cells under study. This result, in combination with the EQE data presented, implies that C_{60} excitons are transferred to the phthalocyanine layer and are subsequently dissociated at the MoO_3 interface, as schematically illustrated in the inset in Figure 6. According to Figure 4, F_{16}ZnPc and C_{60} are not only compatible with regard to excitonic transport, but also in respect to charge carrier transport. Thus, the electrons generated in the phthalocyanine film upon exciton dissociation at the MoO_3-interface can move back to the silver cathode for extraction. Accordingly, F_{16}ZnPc/C_{60} solar cells behave as Schottky cells, with the fullerene acting as sensitizer and electron transport layer.

In literature, the working principle of OPVCs with similar layer sequence was attributed to an exciton recombination process at the F_{16}ZnPc/C_{60} interface in which holes from C_{60} excitons recombine with electrons from excitons created in F_{16}ZnPc.[28] However, our PL measurements are in clear contradiction to this assumption.

The fact that also the electronic transport levels of F_{16}ZnPc and C_{60} are compatible with each other at their common contact offers important implications in the emerging field of, e.g., organic ternary solar cells. Due to the missing energetic offset at this interface, no loss in V_{oc} is expected to occur, since V_{oc} is determined by the outer energy levels of such a cascade or ternary structure.[29] In case of the other solar cells under study, we consider this working mechanism to be negligible, because the energetic offset at the donor/acceptor heterojunction is already favorable for exciton dissociation. Furthermore, the conventional D/A working principle is supported by the exciton density gradient upon dissociation, forcing exciton diffusion within the photoactive layers toward the respective D/A interface.

2.4.2. Investigation of the *j*(*V*) Characteristics

The *j*(*V*) characteristics at AM 1.5 standard illumination intensity are presented in **Figure 7**a, the corresponding cell parameters are summarized for each material combination in Figure 7b. As for the various positions of the participating energy levels a severe impact on the resulting open circuit voltage is expected, we will discuss this quantity at first. For the ZnPc/C_{60} bilayer cells, the measured V_{oc} of 0.51 V coincides with data reported by other groups.[14,30] In case of F_4ZnPc-based bilayer devices, V_{oc} is improved to 0.65 V, which is similar to values of up to V_{oc} = 0.68 V for the corresponding bulk-heterojunction OPVCs.[14] A further increase to V_{oc} = 0.77 V was detected for F_8ZnPc/C_{60} bilayer structures, improving the open circuit voltage with respect to ZnPc/C_{60} bilayer cells by 50%. In contrast, for F_{16}ZnPc/C_{60} a decrease of the open circuit voltage to V_{oc} = 0.41 V is obtained. The V_{oc} values, the corresponding $E_{g,eff}$, and the loss term $\triangle$ according to Equation (2) are summarized in **Table 1**.

The general V_{oc} increase for the F_4ZnPc/C_{60} and F_8ZnPc/C_{60} heterostructures is associated with an effective enhancement of $E_{g,eff}$. For ZnPc/C_{60} and F_4ZnPc/C_{60}, the loss term $\triangle$ is similar with approximately 0.4 eV and is remarkably small in comparison to other OPVCs.[5,7,8] In contrast, for F_8ZnPc/C_{60}-based devices a loss of 0.79 eV is detected. Due to an insufficient energetic offset at the D/A interface (see Figure 5b), exciton dissociation is presumably limited in these devices. Therefore, enhanced recombination losses may take place and lead to the increased discrepancy between eV_{oc} and $E_{g,eff}$.

As discussed in relation to the complementary EQE and PL measurements, F_{16}ZnPc/C_{60} solar cells are based on a different working principle. Excitons generated in both absorber materials, F_{16}ZnPc and C_{60}, are separated at the MoO_3 interface. This explanation is corroborated by the results of the *j*(*V*) characteristics. According to the UPS measurements an effective band gap of 2.0 eV is detected at the F_{16}ZnPc/C_{60} interface. Consequently, it is very unlikely that the phthalocyanine/fullerene interface determines the open circuit voltage of 0.41 V. Instead, we suggest the work function difference of the electrodes to be decisive for the resulting open circuit voltage. This assumption is in accordance with the fact, that in literature a variety of V_{oc} values is published for F_{16}ZnPc/C_{60} bilayer solar cells, depending on the choice of electrode materials.[28,31]

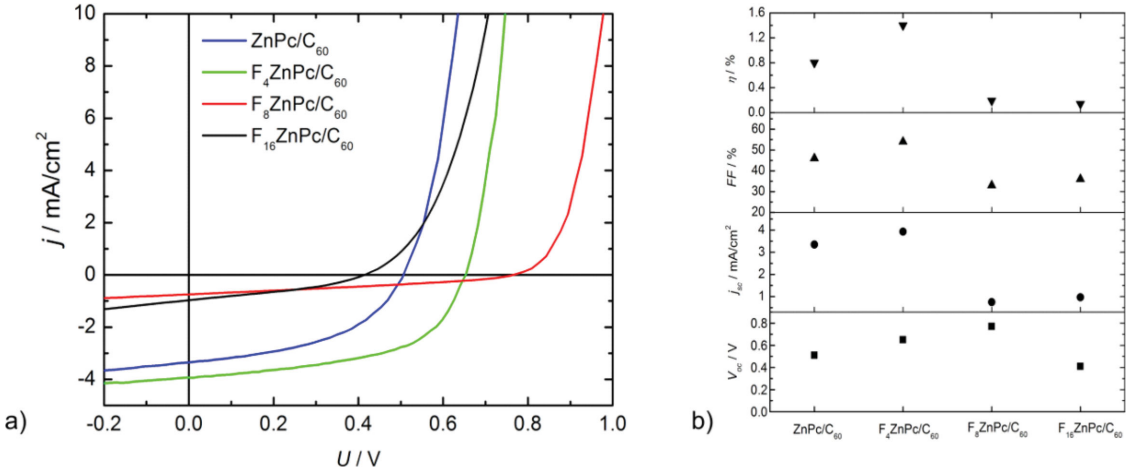

Figure 7. a) $j(V)$ characteristics of F_nZnPc (30 nm)/C_{60} (35 nm) bilayer OPVCs at AM 1.5 standard illumination intensity. b) Summary of corresponding macroscopic device parameters.

Besides significant contributions to the frontier orbital energetics, considerable differences in the short circuit current densities as function of fluorination were observed in accordance with the EQE results. The largest j_{sc} values of 4.0 mA/cm^2 were obtained for F_4ZnPc/C_{60} bilayer cells. This constitutes an increase by about 18% in comparison to ZnPc/C_{60} with j_{sc} = 3.4 mA cm^{-2}. We attribute this improvement predominantly to the higher structural order in the F_4ZnPc layer of the planar heterojunction cells. In accordance with the better transport properties, an enhanced fill factor FF of 55% in comparison to 47% for ZnPc/C_{60} devices can be attested. The short circuit density of the F_8ZnPc/C_{60} bilayer cells amounts to 0.77 mA cm^{-2}. Again, this is attributed to an insufficient energetic offset at the D/A interface preventing exciton dissociation at the organic heterojunction. As indicated by the small fill factor of only 33%, the cell performance is further reduced by the low crystallinity of the F_8ZnPc layer compared to ZnPc or F_4ZnPc. For the F_{16}ZnPc/C_{60} bilayer cells, j_{sc} = 0.98 mA cm^{-2} was measured, i.e., only one fourth of that observed for ZnPc/C_{60} devices. According to the lower spatial extension of crystalline grains, the fill factor of 36% is significantly reduced in comparison to the ZnPc/C_{60} cells.

Finally, as a key criterion for the performance of photovoltaic cells the overall power conversion efficiency η has been evaluated. Though, it was not our primary intention to compete with state-of-the-art OPVC efficiencies but rather to highlight the role interface effects, this parameter provides important insights in the mutual interplay of the individual device parameters and allows to judge the respective device performance with respect to literature data. In this regard, a power conversion efficiency η of 0.81% has been determined for our ZnPc/C_{60} bilayer reference cells, which matches previously published data.[32] As a result of the individually improved solar cell parameters, the highest η of 1.4% is achieved for the F_4ZnPc/C_{60} OPVCs. In contrast, further fluorination yields a decrease in η to 0.19% and 0.14% for the F_8ZnPc/C_{60} and F_{16}ZnPc/C_{60} bilayer devices, respectively.

Table 1. Effective band gap, open circuit voltage, and loss term for OPVCs based on differently fluorinated phthalocyanines. The values for $E_{g,eff}$ and △ for F_{16}ZnPc/C_{60} are listed in brackets, since exciton dissociation predominately takes places at the MoO_3 interface.

Solar cell	$E_{g,eff}$ [eV]	V_{oc} [V]	△ [eV]
ZnPc/C_{60}	0.9	0.51	0.39
F_4ZnPc/C_{60}	1.0	0.65	0.35
F_8ZnPc/C_{60}	1.6	0.77	0.83
F_{16}ZnPc/C_{60}	(2.0)	0.41	(1.59)

3. Conclusion

In summary, we have investigated F_nZnPc thin films and F_nZnPc/C_{60} (n = 0, 4, 8, 16) bilayer photovoltaic cells grown at room temperature and constituting model systems to study the influence of gradual fluorination on the physical properties. XRD measurements showed a significant dependence of the thin film morphology on the degree of fluorination. The long range order, observed in the case of F_4ZnPc/C_{60} bilayer cells, translates into superior transport properties for excitons and free charge carriers, which are indicated by fill factors of 55% and an increase of the short circuit current density by 18% with respect to ZnPc/C_{60} reference cells. Finally, the observed raise of V_{oc} for F_4ZnPc/C_{60} and F_8ZnPc/C_{60} cells by 27% and 50% compared to nonfluorinated ZnPc/C_{60} devices is attributed to an increase of the quasi-Fermi-level splitting at the D/A interface. In contrast, a fundamentally different working mechanism was detected for F_{16}ZnPc/C_{60} solar cells. Both absorber materials are compatible with regard to excitonic and charge carrier transport. This finding offers promising possibilities for the design and implementation in ternary organic photovoltaic cells.

4. Experimental Section

For morphological and optical studies, 40-nm-thick F_nZnPc films were vacuum sublimed. $\theta/2\theta$-scans were performed with an X-ray reflectometer 3003 T/T by GE Inspection Technologies using Cu

$K_{\alpha 1}$-radiation (λ = 1.54056 Å) with an angular resolution of 0.01°. As confirmed by X-ray structural analyses the out-of-plane crystallinity of the 40-nm-thick layers resemble that of the 30-nm-thick films in the bilayer devices.[33] Furthermore, for all bilayer samples, we neither observed an effect of the respective F_nZnPc underlayer on the morphology of the top-grown C_{60} layer nor the formation of a crystalline C_{60} fraction.

Organic photovoltaic cells were prepared on indium tin oxide (ITO) covered glass substrates, neat F_nZnPc thin films on glass substrates. Prior to processing the substrates were cleaned by sonication in acetone and isopropanol for 15 min. Thermal evaporation of the organic layers, metal oxide, and metal layers was carried out in situ in a multichamber vacuum system at a base pressure of 10^{-8} mbar.

For the OPVCs, we used a hole transport layer, consisting of molybdenumoxide (MoO_3) (Mateck). Prior to use, the absorber materials ZnPc and F_{16}ZnPc (Sigma-Aldrich), F_4ZnPc (BASF), F_8ZnPc and C_{60} (Creaphys), were purified twice by thermal gradient sublimation. As an exciton blocking layer we employed Bathophenathroline (BPhen) (Sigma-Aldrich), as received. The top silver electrode was deposited through a shadow mask with a diameter of 2 mm. OPVCs comprised an ITO/MoO_3(5 nm)/F_nZnPc(30 nm)/C_{60}(35 nm)/BPhen(5 nm)/Ag(60 nm) layer structure, which has been optimized to achieve a sufficiently good device performance without shortening the bottom anode and the top cathode. The solar cell parameters were measured in situ, without breaking the vacuum. For measuring the $j(V)$ characteristics, we used a Keithley source measurement unit 236 in combination with a solar simulator LOT Oriel LS0306. The intensity was calibrated to 1 sun at AM1.5 (100 mW cm^{-2}) and was mismatch corrected. For the measurement of the external quantum efficiency, light from a Xe-arc lamp (Osram 150 W/4 Suprasil) was coupled into a monochromator (Oriel Instruments 74100) and focused on the respective OPVCs. The EQE measurements were performed without bias light to avoid photoinduced charge carrier injection and detrapping of charges and at an average light intensity for each wavelength step of $\approx 10^{-2}$ mW cm^{-2} (corresponding to 10^{-4} suns at AM1.5).

In order to investigate the band alignment of the D/A heterostructures, UPS was carried out at BESSY II in Berlin. Metal oxide and organic layers were evaporated from separate Knudsen cells, to prepare the same device architecture (ITO/MoO_3 (5 nm)/F_nZnPc (30 nm)/C_{60} (35 nm)) as in the OPVCs. The UPS measurements were conducted in situ at a base pressure of 2×10^{-9} mbar and at a photon energy of 35 eV with an energy resolution of 50 meV. From the low energy cutoff the vacuum level shift for each layer was determined.

Acknowledgements

This work has been financially supported by the BMBF-project GREKOS (Reference No. 03SF0356A) and within the DFG focus program SPP1355 (Project No. PF385/4-3). J.P. acknowledges the Bavarian State Ministry of Science, Research, and the Arts for generous support within the framework of the Collaborative Research Network "Solar Technologies Go Hybrid."

Received: December 15, 2014
Revised: January 9, 2015
Published online: February 6, 2015

[1] M. A. Green, K. Emery, Y. Hishikawa, W. Warta, E. D. Dunlop, *Prog. Photovolt.: Res. Appl.* **2014**, *22*, 1.
[2] Press release Heliatek, http://www.heliatek.com, accessed: January 2013.
[3] B. A. Gregg, M. C. Hanna, *J. Appl. Phys.* **2003**, *93*, 3605.
[4] L. J. Koster, V. D. Mihailetchi, R. Ramaker, P. W. Blom, *Appl. Phys. Lett.* **2005**, *86*, 123509.
[5] A. Wilke, J. Endres, U. Hörmann, J. Niederhausen, R. Schlesinger, J. Frisch, P. Amsalem, J. Wagner, M. Gruber, A. Opitz, A. Vollmer, W. Brütting, A. Kahn, N. Koch, *Appl. Phys. Lett.* **2012**, *101*, 233301.
[6] K. Vandewal, K. Tvingstedt, A. Gadisa, O. Inganäs, J. V. Manca. *Phys. Rev. B* **2010**, *81*, 125204.
[7] U. Hörmann, J. Kraus, M. Gruber, C. Schuhmair, T. Linderl, S. Grob, S. Kapfinger, K. Klein, M. Stutzman, H. J. Krenner, W. Brütting, *Phys. Rev. B* **2013**, *88*, 235307.
[8] J. Widmer, M. Tietze, K. Leo, M. Riede, *Adv. Funct. Mater.* **2013**, *23*, 5814.
[9] A. Opitz, B. Ecker, J. Wagner, A. Hinderhofer, F. Schreiber, J. Manara, J. Pflaum, W. Brütting, *Org. Electron.* **2009**, *10*, 1259.
[10] D. Schlettwein, K. Hesse, N. E. Gruhn, P. A. Lee, K. W. Nebesny, N. R. Armstrong, *J. Phys. Chem. B* **2001**, *105*, 4791.
[11] I. Bruder, J. Schöneboom, R. Dinnebier, A. Ojala, S. Schäfer, R. Sens, P. Erk, J. Weis, *Org. Electron.* **2010**, *11*, 377.
[12] H. Brinkmann, C. Kelting, S. Makarov, O. Tsaryova, G. Schnurpfeil, D. Wöhrle, D. Schlettwein, *Phys. Status Solidi a* **2008**, *205*, 409.
[13] T. Mayer, U. Weiler, C. Kelting, D. Schlettwein, S. Makarov, D. Wöhrle, O. Abdallah, M. Kunst, W. Jaegermann, *Sol. Energy Mater. Sol. Cells* **2007**, *91*, 1873.
[14] J. Meiss, A. Merten, M. Hein, C. Schuenemann, S. Schäfer, M. Tietze, C. Uhrich, M. Pfeiffer, K. Leo, M. Riede, *Adv. Funct. Mater.* **2012**, *22*, 405.
[15] M. J. Cook, I. Chambrier, *The Porphyrin Handbook* (Eds: K. M. Kadish, K. M. Smith, R. Guilard), Academic, San Diego, CA **2003**.
[16] E. A. Lucia, F. D. Verderame, *J. Chem. Phys.* **1968**, *48*, 2674.
[17] M. I. Alonso, M. Garriga, J. O. Ossó, F. Schreiber, E. Barrena, H. Dosch, *J. Chem. Phys.* **2003**, *119*, 6335.
[18] D. G. de Oteyza, E. Barrena, J. O. Ossó, S. Sellner, H. Dosch, *J. Am. Chem. Soc.* **2006**, *128*, 15052.
[19] A. Ogunsipe, D. Maree, T. Nyokong, *J. Mol. Struct.* **2003**, *650*, 131.
[20] P. Erk, private communication to Cambridge Crystallographic Data Center (CCDC reference code CUPOCY14).
[21] R. R. Lunt, J. B. Benziger, S. R. Forrest, *Adv. Mater.* **2010**, *22*, 1233.
[22] L. D. Siebbeles, A. Huijser, T. J. Savenije, *J. Mater. Chem.* **2009**, *19*, 6067.
[23] A. K. Topczak, T. Roller, B. Engels, W. Brütting, J. Pflaum, *Phys. Rev. B* **2014**, *89*, 201203(R).
[24] S. Krause, M. B. Casu, A. Schöll, E. Umbach, *New J. Phys.* **2008**, *10*, 085001.
[25] R. Murdey, N. Sato, M. Bouvet, *Mol. Cryst. Liq. Cryst.* **2006**, *455*, 211.
[26] A. Kahn, N. Koch, W. Y. Gao, *J. Polym. Sci. B* **2003**, *41*, 2529.
[27] M. S. Golden, M. Knupfer, J. Fink, J. F. Armbruster, T. R. Cummins, H. A. Romberg, M. Roth, M. Sing, M. Schmidt, E. Sohmen, *J. Phys.: Condens. Matter* **1995**, *7*, 8219.
[28] T. Zhang, J. Huang, F. He, L. Chen, G. Niu, J. Pan, Q. Song, *Sol. Energy Mater. Sol. Cells* **2013**, *112*, 73.
[29] K. Cnops, B. P. Rand, D. Cheyns, B. Verreet, M. A. Empl, P. Heremans, *Nat. Commun.* **2014**, *5*, 3406.
[30] Y. Terao, H. Sasabe, C. Adachi, *Appl. Phys. Lett.* **2007**, *90*, 103515.
[31] Q. Song, H. Yang, Y. Gang, C. Gong, C. Li, *J. Am. Chem. Soc.* **2010**, *132*, 4554.
[32] A. Sánchez-Díaz, L. Burtone, M. Riede, E. Palomares, *J. Phys. Chem. C* **2012**, *116*, 16384.
[33] A. A. Zanfolim, D. Volpati, C. A. Olivati, A. E. Job, C. J. Constantino, *J. Phys. Chem. C* **2010**, *114*, 12290.